Res. Rep. Fac. Eng. Mie Univ., Vol. 19, pp. 113-132(1994)

Original Paper

Elasto-Plastic Instability of Restrained Beam-Columns Made of High-Strength Steel

Hideo TAWA, Shosuke MORINO, Jun KAWAGUCHI and Shinya YAMAMOTO†
(Department of Architecture)

(Received September 16, 1994)

Abstract

L-shaped steel frames consisting of an elastic beam and a column were tested under a constant vertical load and varying horizontal load, with the objective to investigate the load-displacement characteristics of beam-columns made of high-strength steel, which were restrained by the beam. The paper presents the test results of specimens failing due to combined effects of lateral-torsional buckling, local buckling and $P\Delta$ moment caused by excessive in-plane displacement, and discusses the load-displacement behavior, the maximum strength and the deformation capacity of the high-strength steel beam-columns, in comparison with the behavior of the mild steel beam-columns. The experimental parameters were shape of H-section of the column, steel grade, column slenderness ratio, stiffness ratio of the beam to the column and axial load ratio to the yield load of the column. It was found that the characteristics of the load-displacement behavior of the high-strength steel specimens were similar to those of the mild steel specimens up to the maximum strength attained, but the strength deterioration of the former caused by combined instability effects was much severer than the latter, which led to less deformation and energy dissipation capacities.

Key words

High-strength steel,Lateral-torsional buckling,Local buckling,Maxinum strength,Deformation and energy dissipation capacities,Numerical analysis

1. Introduction

In the recent high-rise steel building construction, high-strength steel is often used to reduce the cross-sectional area of the column in the lower-story where the axial load ratio be-

†Taiyo Kogyo Corporation

comes prohibitively large. It has been pointed out that the members made of high-strength steel would possess less deformation capacity than those made of mild steel, since the former would become slender than the latter under the same design load. However, the investigation has not been much done, and the quantitative data usable for the design practice are not available. Objective of the research is to investigate the load-displacement characteristics of beam-columns made of high-strength steel.

2. Experimental investigation

2.1 Experiments

Specimen was a simply-supported L-shaped steel frame which consisted of a beam and a column as shown in Fig. 1. The column was a built-up wide flange made of two different steel materials, SS400 and SM570Q, and the beam was made of high-strength steel (HT 80) which remained elastic until the end of the test. Two different cross sections were prepared for the column of the specimen: wide-width H-section and medium-width H-section as shown in Fig. 1. Width-thickness ratios of the flanges of two sections are 11.7 and 5.8, and that of the web is 21.3. The value of 11.7 of the flange is slightly less than the limiting value 12 for SS400, but well exceeds 9.2 (= $12\sqrt{2.4/F}$; F = 4.1) for SM570, specified in the seismic design recommendations in Japan.

Figure 2 is a schematic draw of the loading condition. First, a constant vertical load was applied at the top of the column by a hydraulic jack, and a gradually-increasing horizontal load was applied next by a mechanical screw jack. The top of the column was made free to rotate about three orthogonal axes by a pin. L-shaped specimen was simply supported on a pin and a roller at the base, which were able to rotate in the plane of the specimen frame, and fixed to rotate in the plane perpendicular to the plane of the frame. The axial load P, the horizontal load H and the displacement Δ at the column top were measured by load cells attached at the tips of jacks and a displacement meter, respectively. The longitudinal strain near the base of the column were also measured by the wire strain gauges mounted on the flange and web at the distance about 80 mm apart from the base plate. In M series tests, out-of-plane displacements at 5 points

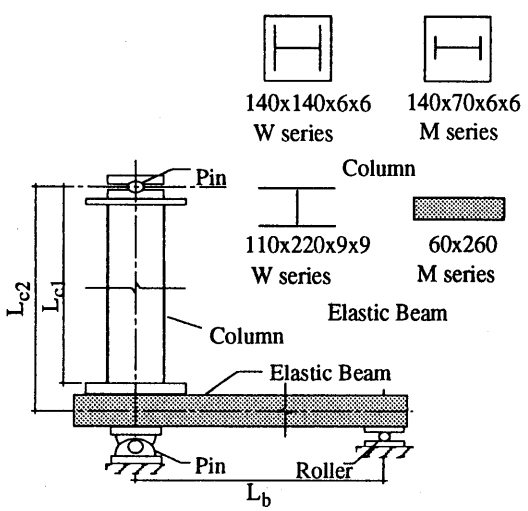

Fig.1 Specimen

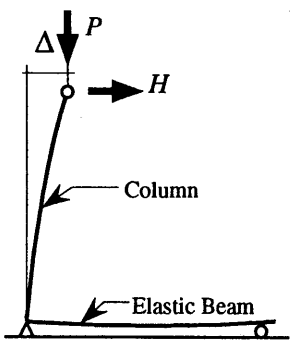

Fig.2 Loading condition

of the column along its length and twisting angle at the top of the column were measured by displacement meters to detect the lateral-torsional buckling deformation.

Experimental parameters were as follows; i) steel grade of the material for the column, ii) shape of the column cross section, iii) slenderness ratio of the column (λ_x), iv) stiffness ratio of the elastic beam to the column (k), and v) axial load ratio of the column to the yield load. Table 1 indicates the values of experimental parameters and specimens tested. The stiffness ratio of the beam k is given by $k = (I_b/L_b)/(I_c/L_{c2})$, where, I and L denote the moment of inertia and the length, respectively, and subscripts b and c indicate the quantities of the beam and the column, respectively. The value of k was controlled by changing the length of the elastic beam L_b.

The name of the specimen indicates the experimental parameters. First letter shows the steel grade of the column material; S for mild-steel and H for high-strength steel. Second letter is for the shape of the cross section: W for wide-width and M for medium-width H-sections. Third letter shows the length of the column; L for the long and S for the short columns. Forth letter is for the stiffness ratio of the elastic beam to the column; A for 0.5 or 0.8, B for 1.5 and C for 3.0. Last two numerals indicate the axial load ratio to the column yield load in %. For example, HWSB30 is a short column specimen of wide-width H-section made of the high-strength steel, with k = 1.5 and the axial load ratio equal to 30 %.

Table 2 shows the measured dimensions of specimens, where L_{c1} and L_{c2} are the distance between the pin at the column top and the upper surface of the base plate or the center line of the beam, respectively, as shown in Fig. 1. The mechanical properties and the stress-strain relations of steel obtained from the coupon tests of mild steel SS400 and high-strength steel SM570Q are shown in Table 3 and Fig. 3, respectively. The yield stress of SM570Q-A for W series was obtained from the 0.2 % off-set method, since it did not exhibit the yield plateau. The materials used for W and M series specimens are quite different, even though they are categorized in the same grade of steel: the value of the yield stress σ_y, the yield ratio Y.R., and the elongation EL. The stress-strain relation of SM570Q-B for M series shows the yield plateau, and its yield ratio is very low as a high-strength steel, which is resulted from a special heat treatment in the rolling process of steel. The tensile strength σ_y of SS400-B for M series is too low, and it does not meet the JIS standards.

Table 1. Experimental parameters

	Material of column		Mild steel (S)						High-strength steel (H)					
	Slenderness ratio of column		λ_x = 25.0			λ_x = 14.9			λ_x = 25.0			λ_x = 14.9		
W Series	Stiffness ratio of beam (k)		0.8 (A)	1.5 (B)	3.0 (C)	0.5 (A)	1.5 (B)	3.0 (C)	0.8 (A)	1.5 (B)	3.0 (C)	0.5 (A)	1.5 (B)	3.0 (C)
	Axial load ratio	10%	○	○		○ *			○	○		○		
		30%	○	○	○	○	○	○	○	○	○	○	○	○
		50%	○			○	○					○	○	
	Material of column		Mild steel (S)						High-strength steel (H)					
	Slenderness ratio of column		λ_x = 26.8			λ_x = 15.9			λ_x = 26.8			λ_x = 15.9		
M Series	Stiffness ratio of beam (k)		0.8 (A)	1.5 (B)	3.0 (C)	0.5 (A)	1.5 (B)	3.0 (C)	0.8 (A)	1.5 (B)	3.0 (C)	0.5 (A)	1.5 (B)	3.0 (C)
	Axial load ratio	10%	○	○		○			○	○		○		
		30%	○	○	○	○	○	○	○	○	○	○	○	○
		50%	○			○	○		○			○	○	

○ specimens tested * 15 %

Table 2. Mesured dimensions (mm)

Specimen	D	W	t_f	t_w	L_{c1}	L_{c2}
HWLA10	140.2	140.0	6.1	5.9	1403.2	1494.2
HWLA30	140.3	139.9	6.5	6.0	1401.9	1492.9
HWLB10	139.7	139.8	6.0	6.1	1403.8	1494.8
HWLB30	140.7	139.9	6.2	6.1	1403.7	1494.7
HWLC30	140.5	139.8	6.3	6.1	1403.2	1494.2
HWSA10	140.4	139.8	6.0	6.1	801.9	892.9
HWSA30	140.8	139.8	6.0	6.1	802.9	893.9
HWSA50	140.3	139.7	6.0	6.1	802.5	893.5
HWSB30	142.1	139.9	6.1	6.0	801.9	892.9
HWSB50	140.5	139.3	6.0	5.8	802.2	893.2
HWSC30	141.2	139.5	5.9	6.3	802.4	893.4
SWLA10	139.5	139.7	6.2	5.9	1400.8	1491.8
SWLA30	138.3	139.3	6.1	6.2	1401.3	1492.3
SWLA50	138.3	138.3	6.0	5.8	1401.3	1492.3
SWLB10	138.7	138.3	6.0	6.0	1401.3	1492.3
SWLB30	137.7	139.3	5.9	6.1	1401.7	1492.7
SWLC30	139.7	138.7	6.0	7.1	1402.3	1493.3
SWSA15	140.4	140.0	6.2	5.6	804.2	895.2
SWSA30	140.7	139.3	6.0	5.9	803.0	894.0
SWSA50	139.3	138.3	6.0	7.4	803.7	894.7
SWSB30	141.2	139.1	6.0	5.9	803.5	894.5
SWSB50	138.0	139.7	6.0	5.9	803.3	894.3
SWSC30	141.1	139.2	6.4	5.8	803.2	894.2
HMLA10	140.2	70.6	6.2	5.8	1399.3	1461.3
HMLA30	141.8	69.9	6.2	6.0	1399.2	1461.2
HMLA50	140.1	70.5	6.0	5.8	1401.2	1463.2
HMLB10	140.5	70.4	6.2	6.3	1400.6	1462.6
HMLB30	140.0	70.3	5.9	5.9	1400.5	1462.5
HMLC30	141.4	70.0	6.1	6.6	1400.3	1462.3
HMSA10	139.6	70.0	6.1	6.0	808.2	870.2
HMSA30	141.2	69.5	6.1	5.9	801.6	863.6
HMSA50	141.8	71.2	6.3	5.9	800.7	862.7
HMSB30	140.7	69.7	6.3	6.0	802.9	864.9
HMSB50	141.3	69.8	6.1	5.9	801.0	863.0
HMSC30	142.0	69.8	6.4	5.9	801.7	863.7
SMLA10	139.9	70.4	5.8	5.9	1399.3	1461.3
SMLA30	140.6	40.5	5.9	5.6	1399.0	1461.0
SMLA50	139.6	70.5	5.9	5.6	1399.8	1461.8
SMLB10	139.6	70.4	5.9	5.8	1399.4	1461.4
SMLB30	140.3	70.1	5.9	5.8	1399.4	1461.4
SMLC30	139.8	70.5	5.9	5.6	1399.4	1461.4
SMSA10	139.5	70.5	5.8	5.9	800.2	862.2
SMSA30	140.2	70.5	6.1	5.8	800.2	862.2
SMSA50	139.6	70.1	5.1	5.7	799.5	861.5
SMSB30	140.5	70.3	5.1	5.9	799.3	861.3
SMSB50	140.3	70.3	5.7	5.8	798.8	860.8
SMSC30	140.1	70.3	5.8	5.8	799.3	861.3

D : Depth of cross section W : Width of cross section
t_f : Thickness of flange plate t_w : Thickness of web plate
L_{c1} ,L_{c2} : Length of the column (see Fig.1)

Table 3. Mechanical properties

	W series		M series	
	SM570Q-A	SS400-A	SM570Q-B	SS400-B
E (kN/mm^2)	190.0	196.0	196.0	193.6
σ_y (N/mm^2)	459.6	309.7	419.4	252.8
σ_u (N/mm^2)	581.1	443.0	589.0	398.7
Y.R. (%)	79.0	69.9	71.2	63.4
EL. (%)	18.0	28.0	21.8	22.8

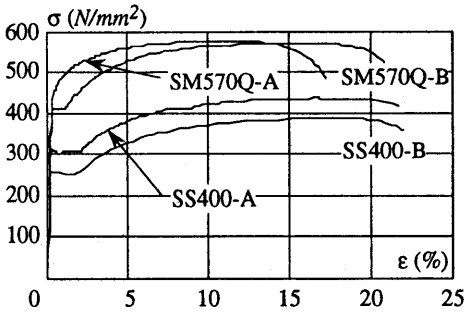

Fig.3 Stress-strain relations

2.2 Experimental results and discussion

(a) Horizontal load-displacement relations

Figures 4 and 5 compare the non-dimensional horizontal load-displacement relations of two corresponding specimens made of mild and high-strength steel. The horizontal load and displacement are divided by H'_{pc} and the displacement Δ_{pc} respectively, which are the strength and the displacement at the intersection of the elastic and the mechanism lines shown by straight lines. The mechanism line is drawn based on the assumption that the plastic hinge forms at the surface of the base plate of the column with the full plastic moment M_{pc} reduced by the axial thrust.

W Series Open and solid triangles in Fig. 4 indicate the points at which the local buckling of flange and web plates were first eye-observed, respectively. The local buckling of flange and web plates of columns were observed in all specimens at the location about 80 mm apart from the base plate, but the load-displacement curves all reach the mechanism lines. Therefore, it may be said that the maximum strength were determined by the full plastic moment M_{pc} of the column and the local buckling did not much affect the maximum strength. The local buckling of the flange plate of the high-strength steel specimens always occurred before the point of the maximum strength (peak point), and occurred earlier compared with the mild steel specimens, in which the flange buckling occurred after the peak point in some cases. The local buckling of the web plate always occurred after the peak point. The strength deterioration after the maximum strength was caused by the $P\Delta$ effect and the web local buckling, and the curves go eventually below the mechanism line. This phenomenon was observed in both the mild steel and the high-strength steel specimens. The negative slopes of the load-displacement curves of the high-strength steel specimens are steeper than those of the mild steel specimens, and they are all steeper than the slope of the mechanism line. The displacement at the occurrence of local buckling becomes smaller with the strength deterioration being severer as each of the axial load ratio, stiffness ratio and slenderness ratio becomes larger.

M Series Figure 5 shows the non-dimensional horizontal load-displacement relations of specimens in M series, where open and solid triangles indicate the points of rapid increase of twisting angle at the column top and of out-of-plane displacement observed, respectively, and an arrow indicates the local buckling of the flange observed. The width-thickness ratio of the flange of M series specimens is rather small, and the local buckling occurred late with the strain

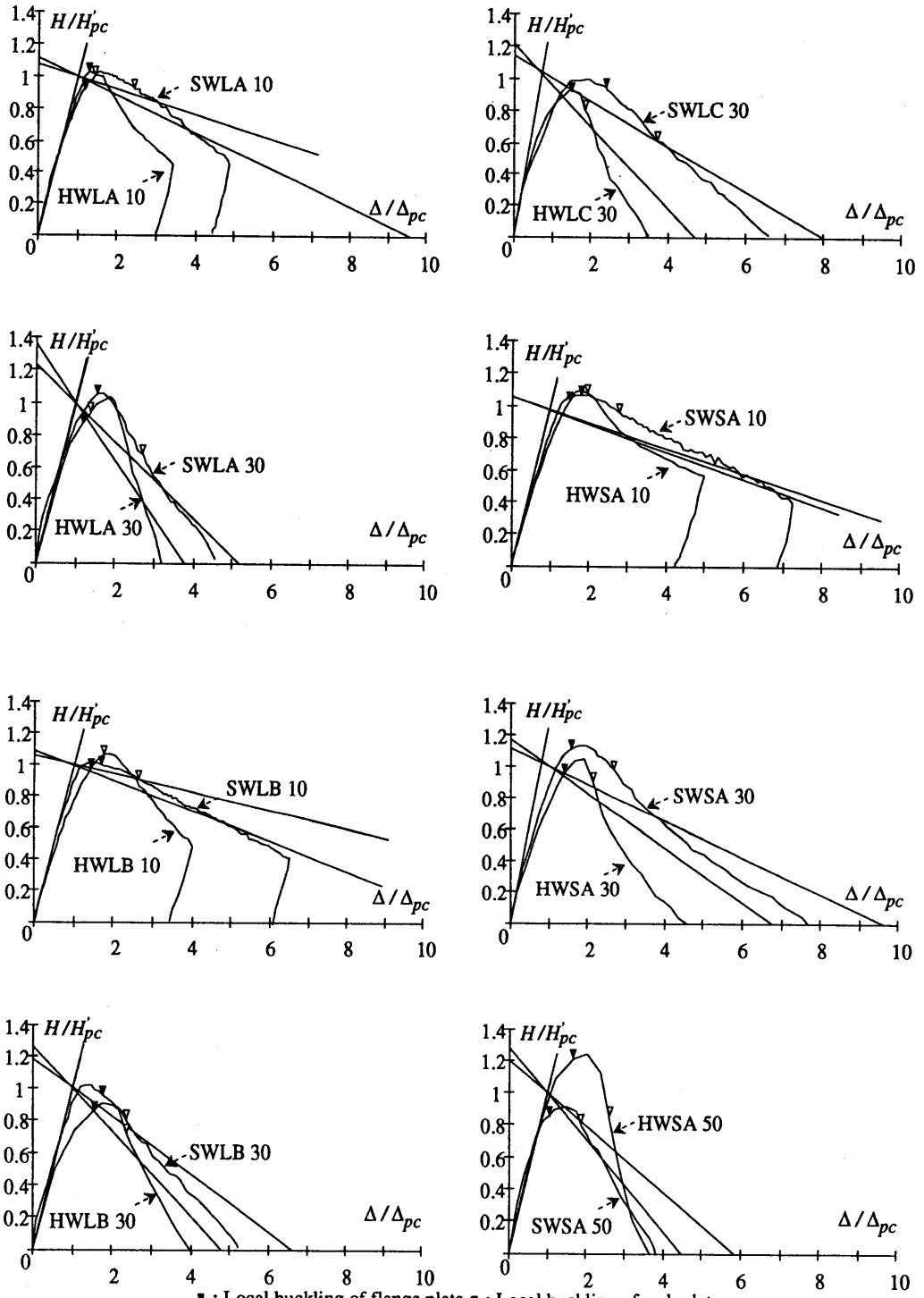

▼ : Local buckling of flange plate ▽ : Local buckling of web plate

Fig.4 Horizontal load-displacement relations (W series)

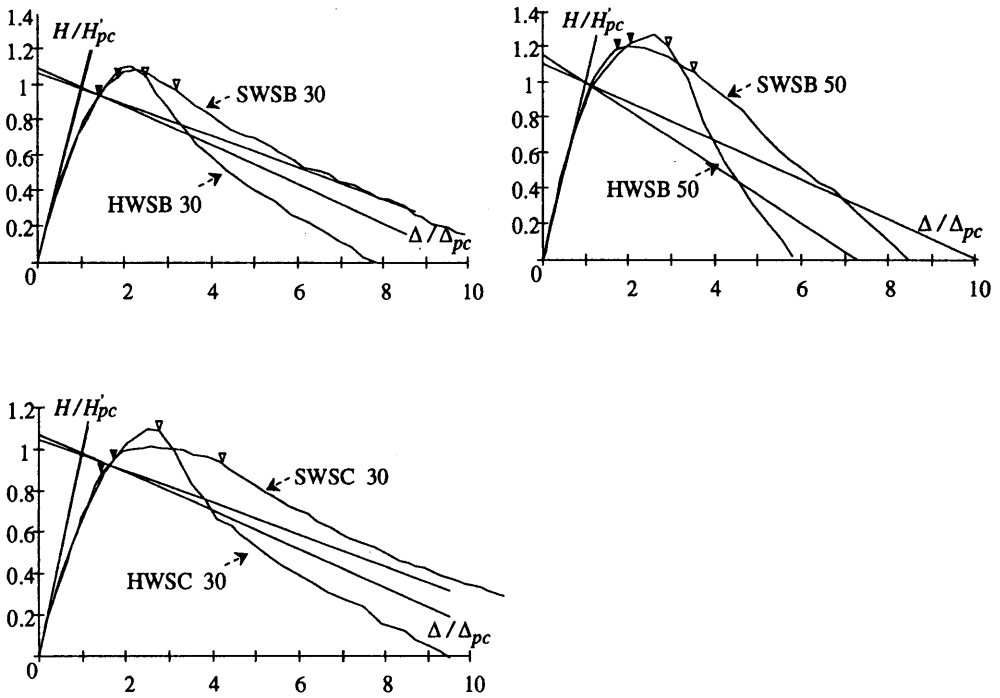

▾ : Local buckling of flange plate ▿ : Local buckling of web plate

Fig.4 Horizontal load-displacement relations (W series) (continued)

of 2 to 3 %, which well exceeds the strain at the start of strain-hardening, 1.15% for high-strength steel and 1.74% for mild steel. Thus, each curve in Fig. 5 largely exceeds the mechanism line due to the strain-hardening effect. The maximum strengths of the M series specimens were determined by the lateral-torsional buckling, which exhibited two patterns of the buckling deformation: the twisting was more pronounced in the specimens subjected to the axial load ratio of 10%, while the out-of-plane deflection was predominant in the case of the specimens subjected to the axial load ratio of 30 and 50%. In general, the strength deterioration after the maximum strength attained was much severer in the high-strength specimens than in the mild steel specimens. This is mainly because the absolute intensity of the axial load is larger in the high-strength steel specimen than in the mild steel specimen, if two specimens under the same axial load ratio are compared, and the local buckling occurred earlier in the former. However, the early strength deterioration in the high-strength steel specimen is also clearly observed in the behavior of HMSA30 in comparison with SMSA50 , and in the behavior of HMSB30 in comparison with SMSB50 , each pair of two specimens being subjected to nearly equal absolute intensity of the axial load.

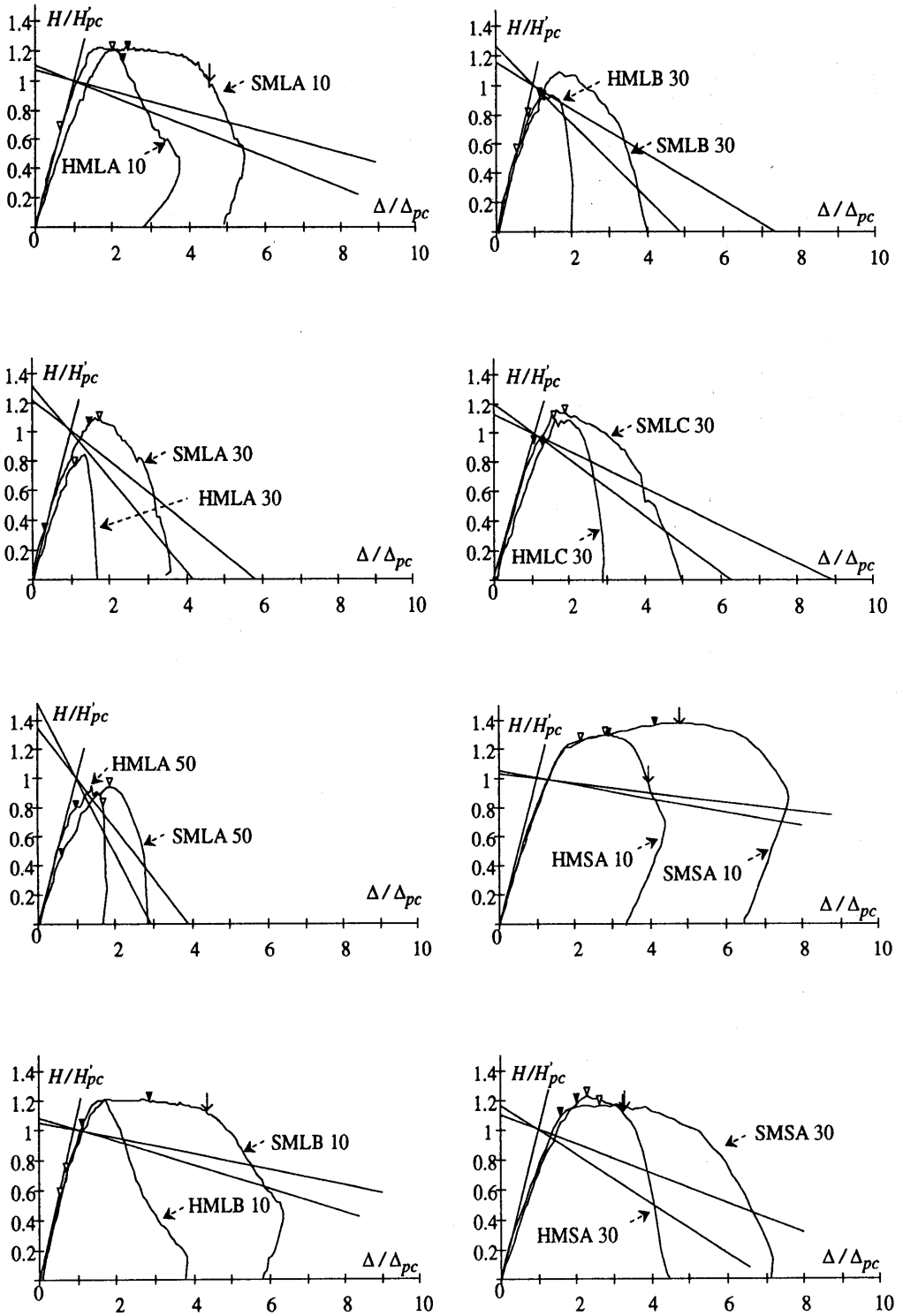

▼ : Out-of-plane displacement
▽ : Twisting angle at the top of column
↓ : Local buckling of flange plate

Fig.5 Horizontal load-displacement relations (M series)

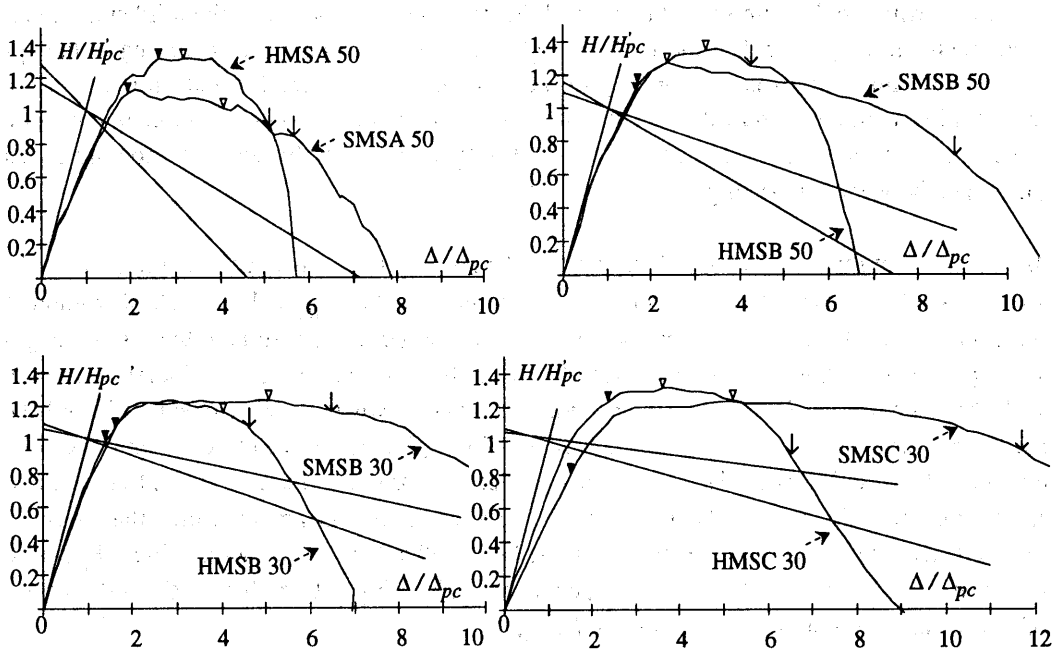

Fig.5 Horizontal load-displacement relations (M series) (continued)

(b) Deformation and energy dissipation capacities

Figure 6 illustrates the definitions of deformation and energy dissipation capacities of steel beam-columns. The deformation capacity is defined by two parameters μ_{max} and $\mu_{0.9max}$ as indicated by the equations in Fig. 6, where $\Delta_{max}$and $\Delta_{0.9max}$are the displacements at which the maximum strength attained and the strength deteriorating to the value equal to 90% of the maximum strength, respectively. On the other hand, the energy dissipation capacity is defined by two plastic deformation factors,$\eta_{pc}$and η_{lp}, which are given as the ratio of the energy dissipated until the maximum strength attained W_2, or the energy dissipated until the the horizontal resistance is exhausted W_3 to the energy dissipated ion the elastic state W_1, as indicated by the equations in Fig. 6. In Figs. 7 and 8, the values of deformation capacity and the values of plastic deformation factor are plotted against the values of P/P_e ,whereP_e denotes the elastic buckling load of the specimen frame. Open and solid squares indicate the test results of the mild and high-strength steel specimens, respectively. Data for the deformation capacity μ are approximated by hyperbolic functions determined by the least squares method: solid and dotted lines for the test results of the mild and high-strength steel specimens, respectively.

W Series In the figures for the deformation capacity m in Fig. 7, the approximation lines by the hyperbolic function are temporarily drawn, but the data seem not showing strong correlation with P/P_e . The maximum strengths of W series specimens were determined by the local buckling, and it is well known that the strength and deformation capacity are quite sensitive with the initial imperfections and invisible microscopic faults existing in the steel plates. This may be

the reason why the data are so scattering, and the deformation capacity of the mild steel specimens seems to be poorer than those of the high-strength steel specimens according to the approximation line, which is the contrary to the common knowledge. The data for the plastic deformation factor η_{pc} indicate that the data for the high-strength steel specimens are more scattering, but the data for η_{lp} decrease with P / P_e hyperbolically, without showing much difference between two steel grades.

M Series Not much difference is observed in the results of μ_{max} between the mild and high-strength steel specimens, but a little difference is observed in $\mu_{0.9max}$ in Fig. 8. The deviation of the data μ from the hyperbolic approximation lines is larger in the results of the high-strength steel specimens. In the region of P/P_eless than 0.05, the deformation capacity increases rapidly with the decrease in P / P_e, but μ becomes less than 2, when P / P_e exceeds 0.2, and the sufficient deformation capacity is not expected in this region due to the effects of initial crookedness and residual stresses. These tendencies appear regardless of the steel grade. In the data of η, it is observed that the results of the high-strength steel specimens more scatter than those of the mild steel specimens, and the latter decrease hyperbolically with the increase in P/P_e ,while the former show a linear relation. Some specimens made of high-strength steel show the values of η less than unity in the region of large P/P_e.

(c) Stability limit strength

Table 4 lists the strengths of all specimens, where H_{max} and H_{pc} denote applied the maximum strength obtained in the tests and rigid-plastic collapse mechanism strength, respectively. H_{ap} is an approximate maximum strength proposed in Ref. [1] based on the investigation of the mild steel beam-columns, which is given as follows:

$$H_{ap} = H_{pc}\left(1 - \frac{2P}{aL_{c1} + P}\right) \qquad (1)$$

where,

a : Elastic horizontal stiffness of L-shaped frame
L_{c1} :Length of the column (see Fig. 1)

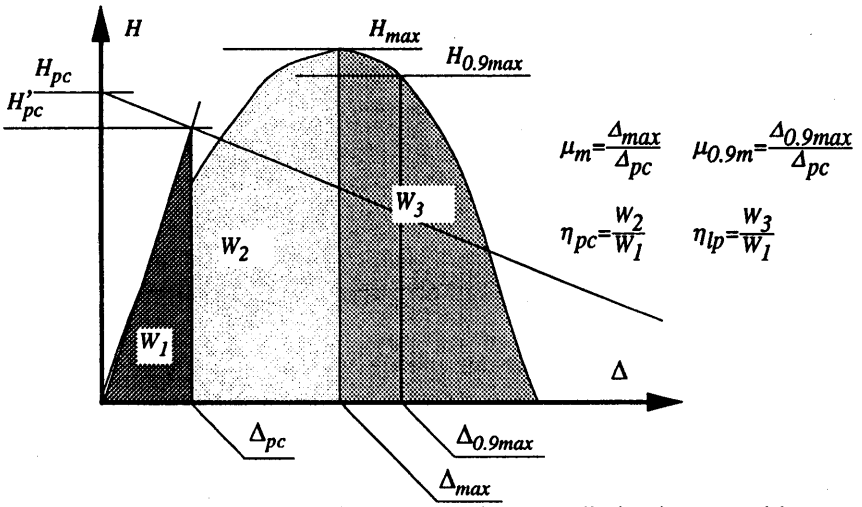

Fig.6 Definitions of deformation and energy dissipation capacities

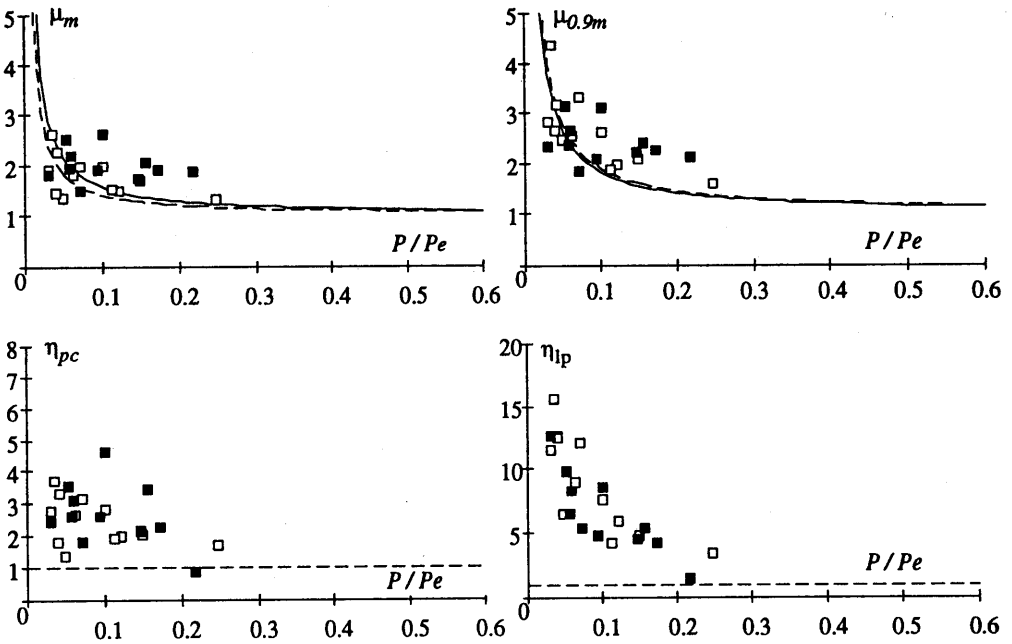

Fig.7 Deformation and energy dissipation capacities (W series)

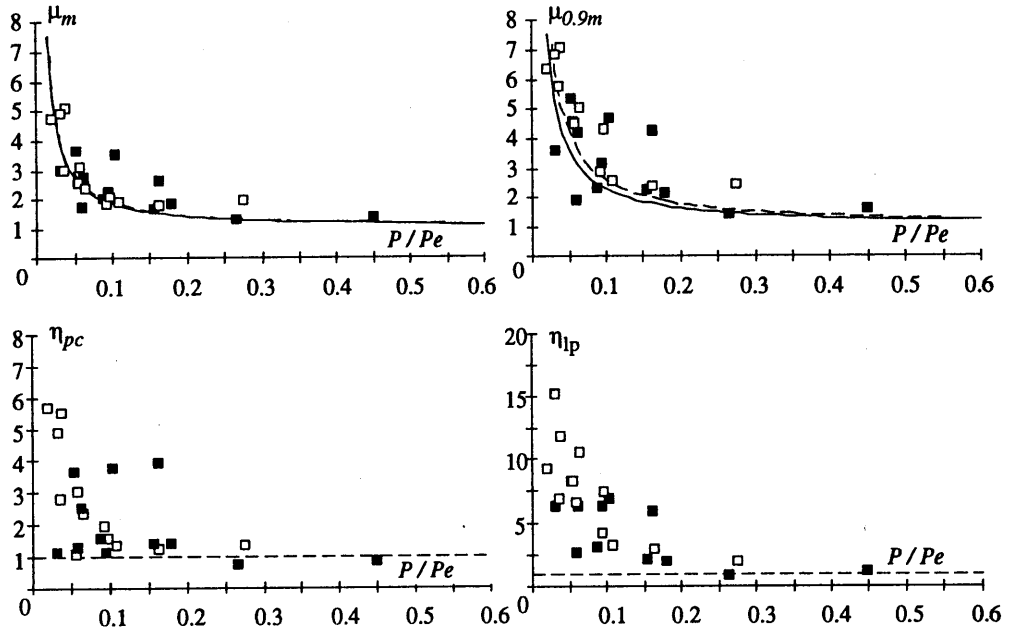

Fig.8 Deformation and energy dissipation capacities (M series)

Figure 9 shows the relation between H_{max}/H_{ap} and P/P_e of all specimens. Solid squares show the results of the high-strength steel specimens and open squares the mild steel specimens.

W Series The values of H_{max}/H_{ap} are larger than unity except it is just unity for one specimen, SWSA50, and Eq. (1) gives the conservative estimate to the maximum strength. It seems that the scatter is rather small in the region of the smaller P/P_e, in other words the smaller λ and larger k, since the effect of the initial imperfection is less. The mean and standard deviation of H_{max}/H_{ap} of the mild steel specimens are 1.127 and 0.099, and those of the high-strength steel specimens are 1.189 and 0.133, respectively, as shown in Table 5. Thus, Eq. (1) gives better estimate to the maximum strength of the mild steel specimens than the high-strength steel specimens.

M Series It is clearly shown that the maximum strengths obtained in the tests well exceed the estimation by Eq. (1), and the value of H_{max}/H_{ap} of the mild steel specimens is constantly about 1.4 regardless of the value of P/P_e, which are somewhat different in comparison with the results of W series. Otherwise similar tendency to W series are observed: The scatter is small in the region of the smaller P/P_e, and Eq. (1) gives better estimates to the maximum strength of the mild steel specimens.

In Fig. 10, the values of H_{max}/H_{ap} are plotted against the values of P/P_e, together with the interaction curves suggested in Refs. [1], [2] and [3]. Merchant [2] gave the linear interaction,

$$\frac{H}{H_{pc}} = 1 - \frac{P}{P_e} \tag{2}$$

and Sakamoto et al. [3] suggested

$$\frac{H}{H_{pc}} = 1 - 0.54\frac{P}{P_e} - 0.46\sqrt{\frac{P}{P_e}} \tag{3}$$

Kimura et al.[1] proposed Eq. (4) based on the investigation of the mild steel beam-columns.

$$\frac{H}{H_{pc}} = 1 - \frac{2\frac{P}{P_e}}{1 + \frac{P}{P_e}} \tag{4}$$

It is observed in Fig.10 that the Merchant's interaction gives unsafe estimate to the maximum strength in some cases, but the other two give conservative values. The mean and standard deviation of the ratio between the experimental maximum strength H_{max} to the strength H_T given by each of the interaction formulas are listed in Table 5. It seems that all the interaction formulas give better estimate to the mild steel specimens and the specimens made of the high-strength steel have larger margin against these estimates. In the region of P/P_e less than 0.15, the difference between H_{max} and H_T becomes larger due to the effects of strain-hardening in *M series* specimens.

Table 4 Test results (kN)

Specimen	P	P_e	P/P_e	H_{max}	H_{pc}	H_{max}/H_{pc}
HWLA10	113.1	1546.7	0.073	41.20	45.57	0.904
HWLA30	356.9	1631.7	0.219	30.28	39.40	0.769
HWLB10	112.1	1922.8	0.058	44.00	44.59	0.987
HWLB30	146.3	1999.6	0.073	27.54	38.32	0.719
HWLC30	348.4	2357.5	0.148	29.50	38.61	0.764
HWSA10	112.0	3584.3	0.031	82.22	78.40	1.049
HWSA30	339.0	3580.6	0.095	58.80	65.37	0.899
HWSA50	562.0	3585.2	0.157	45.57	46.65	0.977
HWSB30	340.9	5647.7	0.060	68.70	66.93	1.026
HWSB50	556.5	5447.6	0.102	51.25	46.35	1.106
HWSC30	337.5	6345.2	0.053	67.82	65.95	1.028
SWLA10	76.8	1570.0	0.049	28.98	30.77	0.942
SWLA30	230.3	1522.1	0.151	20.94	25.09	0.835
SWLA50	370.4	1484.4	0.250	11.62	17.35	0.670
SWLB10	75.0	1768.3	0.042	28.24	29.69	0.951
SWLB30	224.4	1819.9	0.123	20.26	24.40	0.830
SWLC30	239.1	2205.0	0.108	21.82	26.36	0.828
SWSA10	113.7	3593.4	0.032	54.00	53.21	1.015
SWSA30	226.4	3554.0	0.064	44.19	43.90	1.007
SWSA50	399.8	3503.9	0.114	24.42	32.83	0.744
SWSB30	224.4	5374.0	0.042	44.48	43.71	1.018
SWSB50	375.3	5161.0	0.073	33.06	30.58	1.081
SWSC30	233.2	6547.9	0.036	43.75	45.28	0.966
HMLA10	68.1	931.6	0.073	28.03	24.79	1.131
HMLA30	206.8	952.1	0.217	16.85	23.03	0.732
HMLA50	332.2	906.1	0.367	11.86	15.68	0.756
HMLB10	70.7	1173.8	0.060	28.42	25.38	1.120
HMLB30	199.1	1107.4	0.180	20.58	21.95	0.938
HMLC30	213.2	1368.5	0.156	21.66	26.66	0.812
HMSA10	69.5	2678.0	0.026	54.09	41.80	1.294
HMSA30	207.8	2670.8	0.078	42.88	34.98	1.226
HMSA50	343.2	2580.4	0.133	29.57	22.52	1.313
HMSB30	208.8	3297.6	0.063	45.35	36.93	1.228
HMSB50	342.8	3291.7	0.104	33.99	25.09	1.355
HMSC30	205.9	3832.9	0.054	49.10	37.37	1.314
SMLA10	39.8	711.2	0.056	16.17	14.21	1.138
SMLA30	118.0	719.5	0.164	11.76	13.03	0.903
SMLA50	195.5	707.3	0.276	7.55	9.21	0.820
SMLB10	39.5	1072.6	0.037	16.45	14.21	1.158
SMLB30	119.0	1088.9	0.109	12.45	13.13	0.948
SMLC30	122.0	1255.3	0.097	13.33	12.94	1.030
SMSA10	39.5	2020.0	0.020	33.25	24.13	1.378
SMSA30	119.4	2031.1	0.059	24.66	21.08	1.170
SMSA50	196.2	1993.1	0.098	16.00	14.21	1.126
SMSB30	117.8	3048.6	0.039	26.78	21.72	1.233
SMSB50	196.6	3035.1	0.065	19.04	15.03	1.267
SMSC30	118.3	3552.7	0.033	26.97	21.91	1.231

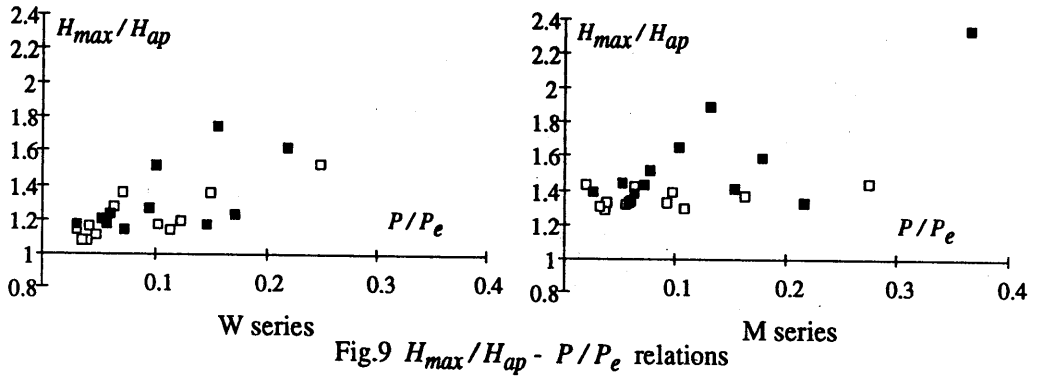

Fig.9 H_{max}/H_{ap} - P/P_e relations

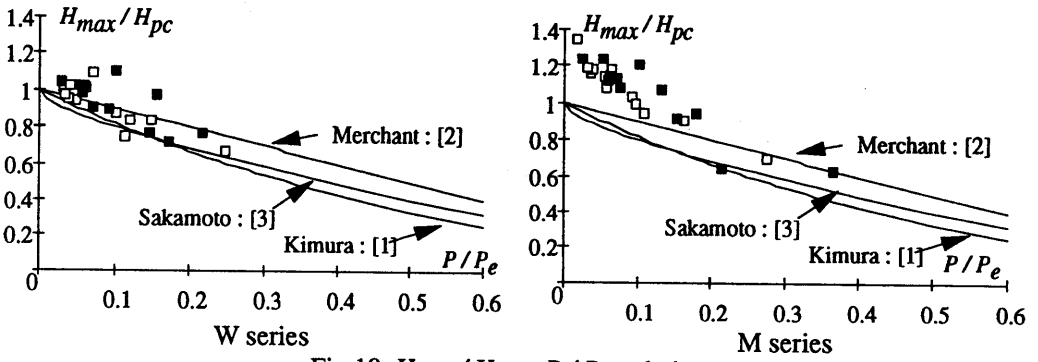

Fig.10 H_{max}/H_{pc} - P/P_e relations

Table 5 Accuracy of strength interraction formulas

		H_{max}/H_{ap}		H_{max}/H_T					
				Merchant		Sakamoto		Kimura	
		SM570Q	SS400	SM570Q	SS400	SM570Q	SS400	SM570Q	SS400
W series	mean	1.310	1.210	1.030	0.997	1.155	1.107	1.137	1.084
	Standard deviation	0.210	0.139	0.105	0.085	0.113	0.082	0.112	0.077
M series	mean	1.554	1.347	1.163	1.164	1.309	1.287	1.301	1.259
	Standard deviation	0.293	0.056	0.147	0.107	0.140	0.083	0.119	0.059

3. Theoretical investigation

3.1 Analysis of beam-columns failing in local buckling

The elasto-plastic behavior of beam-columns is analyzed based on the degrading type stress-strain relations which deal with the strength deterioration due to the effect of local buckling. The stress-strain curve assumed for the steel is shown in Fig. 11(a), where the points P, Y and U indicate proportional limit, start of strain-hardening in tension and occurrence of local buckling in compression, respectively. The curve consists of linear elastic (point P_t to P_c), curvilinear elasto-plastic transition (point P_t to Y and point P_c to U), strain-hardening (point Y to T) and strength deterioration (point U to C) parts. They are given by the following mathematical expressions:

Elastic part $\sigma(\varepsilon) = E \times \varepsilon$ (5)

Transition part $\sigma(\varepsilon) = \sigma_1(\varepsilon) + \sigma_2(\varepsilon)$ (6)

where

$$\sigma_1(\varepsilon) = \frac{(\varepsilon - \varepsilon_{pt}) \times (\sigma_y - \sigma_{pt}) / (\varepsilon_y - \varepsilon_{pt})}{\left[1 + \{(\varepsilon - \varepsilon_{pt}) / (\varepsilon_y - \varepsilon_{pt})\}^k\right]^{\frac{1}{k}}} + \sigma_{pt} \quad (7)$$

$$\sigma_2(\varepsilon) = \frac{\sigma_y - \sigma_1(\varepsilon_{st})}{(\varepsilon_{st} - \varepsilon_{pt})} \times (\varepsilon - \varepsilon_{pt})$$

Hardening part $\sigma(\varepsilon) = E_{st} \times (\varepsilon - \varepsilon_{st}) + \sigma_y$ (8)

Deterioration part $\sigma(\varepsilon) = \left\{\sqrt{(4\lambda^2 F^2(\varepsilon) + 1)} - 2\lambda F(\varepsilon)\right\} \times \sigma_u$ (9)

where

$$F(\varepsilon) = \sqrt{\{2 \times (\varepsilon - \varepsilon_{cr}) + (\varepsilon - \varepsilon_{cr})^2\}} \quad (10)$$

$$\lambda = ND/t \quad (11)$$

Equation 7 is written for the curve in compression, and subscript pc should read pt, u should read y, and cr should read st, for the curve in tension. The values of k should be different for compression and tension. Equations (6) and (7) are derived by modifying an equation proposed by Richard[4], in which the parameter k determines the shape of the curve: the curve approaches the ideal elasto-plastic type shape with the increase of k, and the curvature of the curve becomes larger as k becomes smaller, as shown in Fig. 11(b). On the other hand, the parameter N determines the shape of the curve of the deterioration part as shown in Fig. 11(c). Those parameters appearing in the equations above are determined from the coupon test in tension and the stub column test in compression, and listed in Table 6. Equation (9) is derived in view of a technique to replace a locally-buckled plate by a number of buckled bars shown in Ref.[5]. Note that the stress-strain relation shown above includes the effect of local buckling in a macroscopic way. It is not for an infinitesimal element, but it should be defined as the force-deformation relation of a bar element with unit area and finite length.

The moment-curvature relation is numerically obtained by separating the flange and web of the H-section into a number of elements, each of which follows the stress-strain relations assumed as above. The moment-curvature relation determined in such a way becomes a deteriorating type, and thus a conventional numerical integration scheme cannot be applied to analyze the load-displacement relations. Therefore, in the present analysis, the beam-column is modelized on the assumptions that it is fixed at the base, the deformable portion is concentrated at the base, in which the curvature corresponding to the bending moment generated at the base is uniformly distributed, and the rest of the beam-column is rigid. The length of the deformable portion is determined so that the elastic displacement at the top of this model coincides with the exact solution, that is equal to $(1 - 1/\sqrt{3})$ times L_{c2} in Fig. 1.The load-displacement relation of an L-shaped frame as tested is obtained by superposing the top deflection caused by the rotation generated at the beam end corresponding to the moment of the column base on the relation calculated for the beam-column above. The analysis considering the effect of local buckling is performed for W series specimens only, since the local buckling occurs quite late in the case of M series.

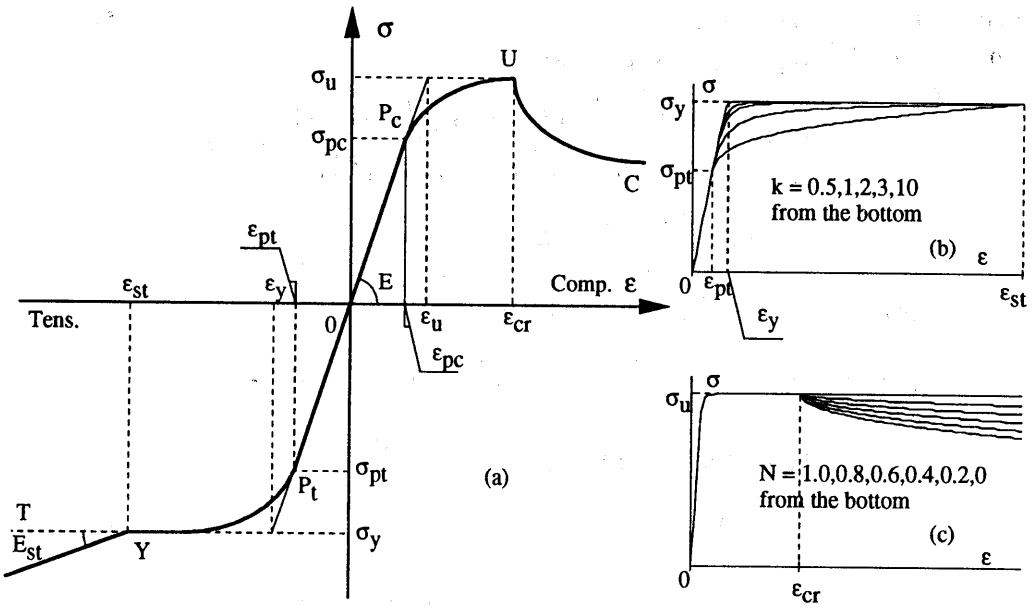

Fig.11 Stress-strain relations for analysis

Table 6 Parameters for stress - strain relations

	W series		M series	
	SM570Q	SS400	SM570Q	SS400
E (kN/mm^2)	235.0	196.0	196.1	193.6
Est/E	0.014	0.012	0.022	0.015
σ_{pt} (N/mm^2)	306.4	309.7	419.4	252.8
σ_y (N/mm^2)	465.2	309.7	419.4	252.8
$\varepsilon_{st}/\varepsilon_y$	2.43	13.1	5.37	13.28
k (tens.)	2.0	10.0	10.0	10.0
σ_{pc} (N/mm^2)	169.8	142.1	419.4	252.8
σ_u (N/mm^2)	459.6	329.3	570.4	387.1
$\varepsilon_{cr}/\varepsilon_y$	3.63	4.81	9	16
k (comp.)	1.25	2.0	2.0	2.0
N	0.093	0.056	1.0	1.0

3.2 Analysis of beam-columns failing in in-plane instability

The load-displacement relations of specimens tested are analyzed by the numerical integration scheme without considering the effect of local buckling. The model for the beam-column in this case is a cantilever subjected to a vertical load P and a horizontal load H at the top as shown in Fig. 12(a). It is separated into n segments longitudinally, and the equilibrium of (i+1)th segment with the length a is written as follows, referring to Fig. 12(b):

$$M_i - M_{i+1} + Q_{i+1}\, a + P\,(y_{i+1} - y_i) = 0 \qquad (12)$$

where $Q_{i+1} = H$. From the equilibrium of the total cantilever,

$$M_0 = -P\Delta - H\,L_{cl} \qquad (13)$$

The central difference expression of the curvature at the nodal point i is given by

$$\phi_i = -\frac{y_{i+1} - 2\,y_i + y_{i-1}}{a^2} \qquad (14)$$

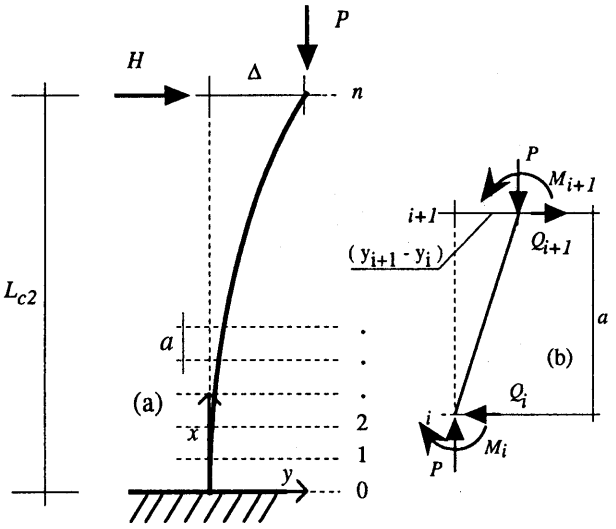

Fig.12 Analytical model for numerical integration

The numerical integration scheme is as follows: First, a trial value is assumed for the bending moment at the base M_0 for a given value of the horizontal displacement at the top Δ, and the horizontal force H is tentatively determined. Suppose the integration proceeds to the nodal point i and all quantities M_i, y_i and ϕ_i have been determined. The horizontal deflection y_{i+1} and then the bending moment M_{i+1} are determined from Eqs. (14) and (12), respectively. The curvature ϕ_{i+1} corresponding to M_{i+1} is determined from the moment-curvature relation prepared a priori. Repeating this procedure up to the top of the cantilever, the top deflection y_n is finally obtained. If the value of y_n is sufficiently close to the value of Δ tentatively determined at the beginning, converged solution is obtained. Otherwise, the procedure should be re-started with another trial value for M_0. As mentioned in Section 3.1, the load-displacement relation of L-shaped flame is obtained by superposing the elastic beam deflection on the result of the beam-column analysis.

In order to apply the numerical integration explained above, the moment-curvature relation must be stable, and thus it is calculated assuming that the material follows the stress-strain relation defined by Eqs. (5) through (8) with the parameters in Table 6 for tension, in the case of the analysis for W series specimens. In the case of M series, the occurrence of the local buckling is quite delayed, and the strength in compression goes up higher due to the strain-hardening effect. In order to take this phenomenon into account, the stress-strain relation for compression is artificially generated as follows: First the value of σ_{pc} is taken equal to σ_y for tension, and the values of σ_u and ε_{cr} are set by multiplying σ_y and ε_y by certain factors, respectively. ε_{cr} is considered as the strain at the occurrence of local buckling, although the strength deterioration is not considered, and the stress sustains the value of $\sigma_u$after the strain exceeds the value of ε_{cr}. This treatment is based on the test data reported in Ref. [6]. Table 6 lists the values for the parameters appearing in the stress-strain relations assumed in the analysis.

3.3 Theoretical results and discussion

Figures 13 and 14 compare the results of analysis with the test results of typical specimens under the axial load ratio of 30% in W and M series, respectively, where thick line indicates the test results, and thin line the results of analysis. Two curves of the analysis are shown for W series specimens in Fig. 13, and the curve II is the results of analysis considering the local buckling effect.

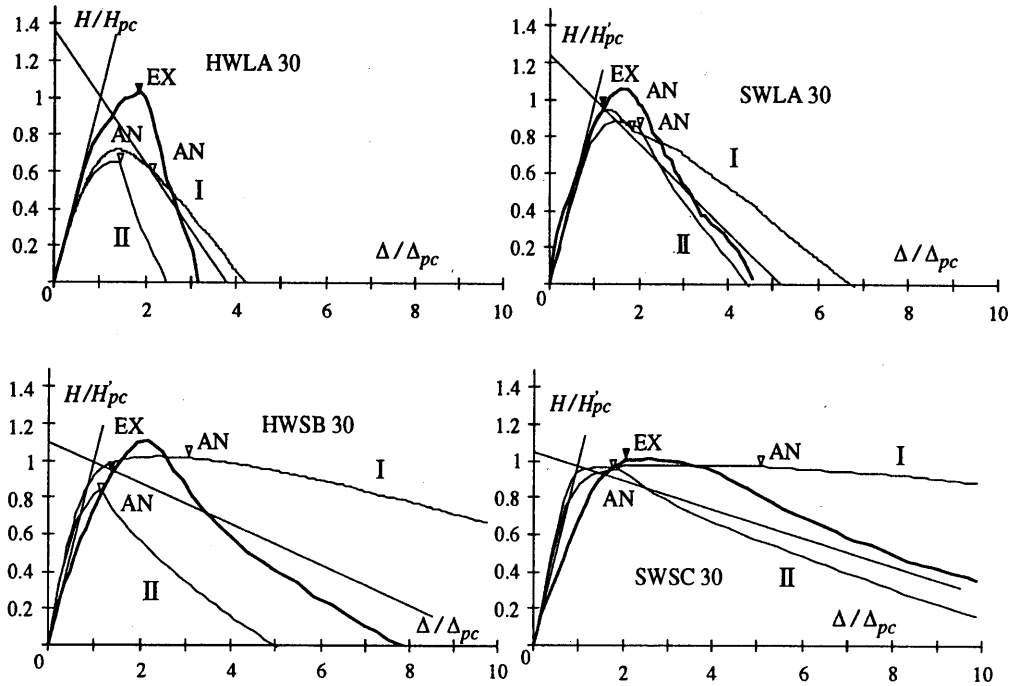

Fig.13 Results of analysis (W series)

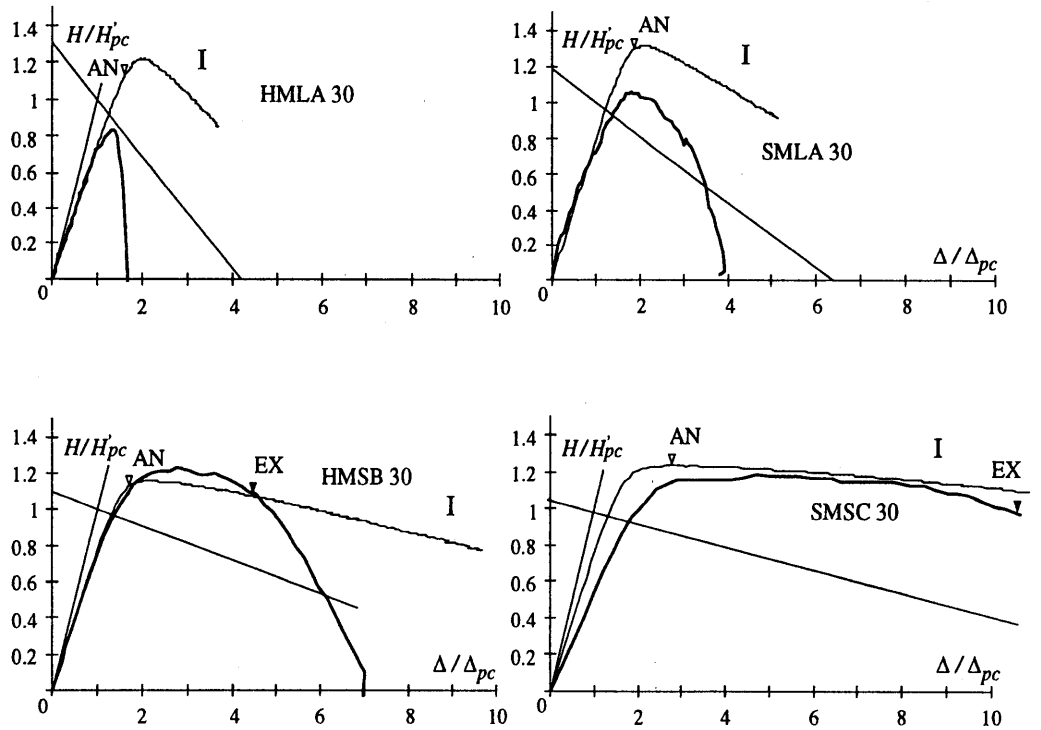

Fig.14 Results of analysis (M series)

W Series The analysis not considering the local buckling effect (curve I) well traces the test results up to the maximum strength, and the analytical strength much exceeds the test results due to the strain-hardening in the former and the local buckling in the latter. The maximum strength

is well estimated by this analysis. On the other hand, the maximum strength given by the analysis considering the local buckling effect (curve II) is much lower than that obtained in the test due to the analytical model with a deformable portion concentrated at the base. However, the shape of the unloading curve after the maximum strength attained very well coincides with the test results. These general tendencies are observed in both mild and high-strength steel specimens. The difference between the maximum strengths obtained in the test and the analysis II are much larger in the high-strength steel specimens.

M Series The point marked as AN in Fig. 14 indicates the point at which the strain in the critical section reaches the strain set for the occurrence of local buckling ε_{cr}, although strength deterioration is not considered in the analysis as mentioned before. The point EX is the point at which the local buckling was observed by eyes in the tests. In the case of long-column specimens, the out-of-plane deflection reduces the maximum strength, and thus the analysis not considering the lateral-torsional buckling over-estimates the strength observed in the tests. However, the analysis very well traces the test results of short-column specimens until the local buckling occurs. The occurrence of the local buckling is much earlier in the analysis than in the tests, since the analysis assumes the critical section at the column base, while the actual local buckling occurs at the section at a certain distance apart from the base.

4. Concluding remarks

Behavior of W series specimens

a) Specimens made of high-strength steel showed quite similar horizontal load-displacement characteristics to the mild steel specimens under variety of experimental parameters. However, the strength deterioration after the maximum strength caused by $P\Delta$ effect and the local buckling of the web were severer than the mild steel specimens.

b) The local buckling of the flange plate of the high-strength steel specimens always occurred before the point of the maximum strength, which is earlier compared with the mild steel specimens. The local buckling of the web plate always occurred after the point of the maximum strength.

c) The data for the deformation capacity seem not showing strong correlation with the axial load ratio to the elastic buckling load, since the maximum strengths are determined by the local buckling. However, the data for the plastic deformation factor η_{lp} decrease with the axial load ratio hyperbolically, without showing much difference between two steel grades.

Behavior of M series specimens

d) The local buckling occurred late, well exceeding the start of strain-hardening, and thus each curve largely exceeds the mechanism line. The maximum strengths were determined by the lateral-torsional buckling, which exhibited two patterns of the buckling deformation: the twisting was more pronounced, or the out-of-plane deflection was predominant.

e) In general, the strength deterioration after the maximum strength attained is much severer in the high-strength steel specimens than in the mild steel specimens.

f) The deviation of the data of the deformation capacity from the hyperbolic approximation line is larger in the results of the high-strength steel specimens. The data of the plastic deformation factor of the high-strength steel specimens more scatter than those of the mild steel specimens,

and the latter decreases hyperbolically with the increase in the axial load ratio.

Results of analysis

g) Conservative estimate to the maximum strength is obtained by Eq. (1), and it gives better estimate to the maximum strength of the mild steel specimens than the high-strength steel specimens. This tendency is also observed in the deviations of the maximum strength from the strengths given by the interaction formulas proposed elsewhere.

h) The maximum strengths of W series specimens given by the analysis considering the local buckling effect are much lower than those obtained in the test due to the analytical model with a deformable portion concentrated at the base. However, the shape of the unloading curve very well coincides with the test results.

i) The analysis not considering the lateral-torsional buckling over-estimates the strength of long-column specimens in M series which is affected by the out-of-plane deflection. However, the analysis very well traces the test results of short-column specimens until the local buckling occurs.

Acknowledgements

The experimental study presented here is a part of the joint research project "Strength and Deformation Capacity of Steel Beam-Columns", supported by the Grant-In-Aid for Scientific Research, Ministry of Education, Japan (Research representative : Shosuke Morino). The authors wish to express their sincere gratitude to Nagoya Works of Nippon Steel Corporation and NKK Corporation for providing the high-strength steel material, and to Messrs. Yutaka Ohmine (Kajima Corporation), Hideo Moriyoshi (Mie Prefectural Office), Takashi Nishikubo (Showa Consultants) and Norio Manabe (Mie University) for their help in the experimental work.

References

[1] Kimura, J., Tomoda, M., Matsui, C. and Morino, S.: Stability Limit Strength of Steel Subassemblages, Transactions of the Architectural Institute of Japan, Journal of Structural and Construction Engineering, No. 433, pp. 51-60, 1992.5.

[2] Merchant, W.: The Failure Load of Rigid Jointed Frameworks as Influenced by Stability, The Structural Engineer, Vol. 32, No. 7, pp. 185-190, 1954.7.

[3] Sakamoto, J., Miyamura, A. and Watanabe, M.: Effect of Strain-Hardening on Steel Structure, Transactions of the Architectural Institute of Japan, No. 134, pp. 9-17, 1967.4.

[4] Smith, J. H.: Nonlinear Beam and Plate Elements, Proc. of ASCE, Journal of Structural Division, Vol. 98, No. ST3, pp. 555-571, 1972.3.

[5] Morino, S., Matsui, C. and Yoshikai, S.: Local Buckling of Steel Elements in Concrete Encased Columns, Proceedings of Pacific Structural Steel Conference, Vol. 2, pp. 319-335, 1986.8.

[6] Yamada, S., Akiyama, H. and Kuwamura, H.: Deteriorating Behavior of Wide Flange Section Steel Members in Post Buckling Range, Transactions of the Architectural Institute of Japan, Journal of Structural and Constructional Engineering, No. 454, pp. 179-186, 1993.12.